energy&fuels

Article

pubs.acs.org/EF

Numerical Study of NO_x Emissions from *n*-Heptane and 1-Heptene Counterflow Flames

Xiao Fu, Stephen Garner, Surresh Aggarwal,* and Kenneth Brezinsky

Department of Mechanical and Industrial Engineering, University of Illinois at Chicago, 842 West Taylor Street, Chicago, Illinois 60607, United States

ABSTRACT: Several engine studies have observed higher amounts of nitric oxide (NO) during the combustion of biodiesel fuels than from regular diesel. One hypothesis for the increased NO formation is that unsaturated components in biodiesel fuels produce higher amounts of acetylene, especially during fuel-rich oxidation, which results in higher prompt NO. In this study, we examine this hypothesis by considering partially premixed flames (PPFs) in an opposed jet configuration, burning prevaporized *n*-heptane and 1-heptene fuels, which represent the hydrocarbon side chain of the two surrogate biodiesel esters, methyl octanoate (C9:0) and methyl octenoate (C9:1), respectively. The configuration involves two opposing jets, one containing a fuel−air mixture issuing from the bottom nozzle and the other containing air issuing from the top nozzle. It provides a nearly one-dimensional flat flame for detailed measurements and simulations and is well-suited for fundamental investigations of kinetics and transport processes. Using a comprehensive chemistry and transport model, PPFs are simulated for a range of equivalence ratios (ϕ). Results indicate that the β-scission and oxidation reactions related to the C=C double bond lead to a higher amount of C_2H_2 and, thus, increased NO through the prompt mechanism in 1-heptene flames compared to that in *n*-heptane flames. However, differences in the NO formation between the two fuels become less noticeable as the level of partial premixing is reduced or as ϕ is increased toward the diffusion flame limit. In addition, analysis of the various NO production pathways indicate that the total NO formed is mainly due to the prompt NO and intermediate N_2O mechanisms, followed by the NNH and thermal NO mechanisms.

1. INTRODUCTION

Biodiesel fuels are commonly produced via the esterification process by transforming vegetable oil or animal fat through reactions with alcohol (such as methanol) in the presence of either an acid or a base catalyst.[1,2] Common types of vegetable-oil-based biodiesel fuels include methyl esters made from canola, coconut, palm, peanut, soy, and rapeseed oils. Their chemical composition and properties vary over a wide range depending upon the source and process used to make the fuel. Consequently, their atomization, combustion, and emission characteristics can also vary significantly. Despite the wide variation in their chemical and physical properties, previous studies have provided strong evidence that biodiesel represents a cleaner alternative to conventional diesel.[1] Figure 1 adopted from a National Renewable Energy Laboratory (NREL) report[3] shows that the emissions of CO, NO_x, and particulate matter are measurably reduced from biodiesel combustion compared to those from conventional diesel combustion. However, there is generally an increase in NO_x from the combustion of biodiesels, as indicated by several engine studies. According to a comprehensive United States Environmental Protection Agency (U.S. EPA) report,[4] the average increases in NO_x for a 20% biodiesel blend and neat biodiesel are 2 and 10%, respectively. These data are supported by experimental studies; see, for instance, one reported by Mueller et al.,[5] who observed a 4−14% increase in NO_x, depending upon engine load, for neat biodiesel compared to conventional diesel. Several other studies[6−8] have examined the NO_x characteristics of biodiesel fuels and observed a correlation between the formation of NO_x and the iodine number. Because the iodine number is a measure of the degree of unsaturation, i.e., number of double bonds in the molecular structure, it has been suggested that the increased NO_x production is due to the chemical consequences and not simply the physical effects of the double bonds in higher iodine number biodiesel fuels.[9,10]

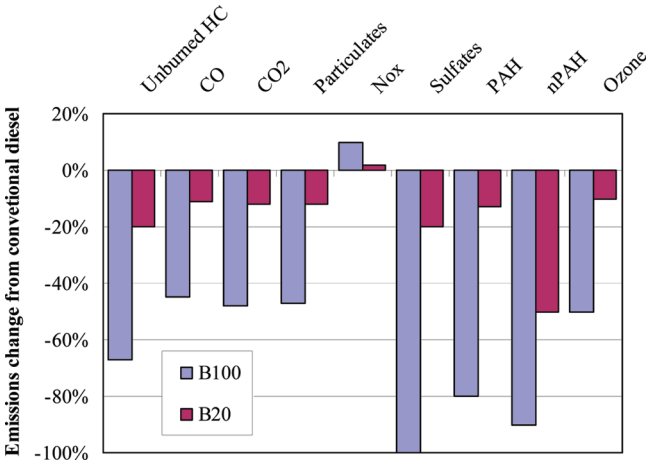

Figure 1. Change in emissions with biodiesel from conventional diesel.[3] B100, 100% biodiesel; B20, 20% biodiesel + 80% conventional diesel.

Because biodiesels are blends of several components, previous studies have used different surrogates for examining

Received: September 19, 2011
Revised: January 11, 2012
Published: January 11, 2012

their combustion and emission characteristics. Studies dealing with short-chain biodiesel surrogates, such as methyl butyrate and methyl butenoate, indicated that the saturated hydrocarbon, ethane, produces more NO than ethene, implying that short-chain biodiesel fuels may not be a good choice to study the effects of the fuel molecular structure on NO.[11−14] Garner et al.[15] performed shock tube pyrolysis experiments using *n*-heptane and 1-heptene as analogues for the saturated and unsaturated hydrocarbon side chains of C_8 methyl esters and observed that 1-heptene produces more acetylene (C_2H_2) than *n*-heptane over intermediate temperatures (1100−1600 K). Garner et al.[16,17] further demonstrated, by the use of a detailed kinetic model of the rich oxidation of C_8 methyl esters, the coupling between the increased acetylene, formed from unsaturated fuels, and the higher prompt NO formed under rich oxidation conditions over the same intermediate temperatures (1100−1600 K). This temperature regime is of relevance to diesel combustion and is also the regime where prompt NO is one of the dominant contributors to the observed NO levels.[12,18] However, previous studies have not examined these aspects in flames, especially in partially premixed flames (PPFs). For *n*-heptane flames, the prompt NO has been found to be the major contributor to the total NO in PPFs.[18−20]

In this work, PPFs have been simulated in an opposed jet flow configuration using *n*-heptane and 1-heptene fuels, which represent the hydrocarbon side chain of the two surrogate biodiesel esters, methyl octanoate (C9:0) and methyl octenoate (C9:1), respectively. The objective is to employ a realistic flame environment and examine the hypothesis that the oxidation of unsaturated long-chain hydrocarbons results in increased NO formation and is due to the prompt NO mechanism. In addition, contributions of the various NO formation routes, such as thermal, prompt, intermediate N_2O, and NNH routes, to the total NO_x formation are characterized. The paper is organized as follows. The numerical model for simulating PPFs is briefly described in section 2. Section 3.1 describes the results of a validation study and the global structures of *n*-C_7H_{16} and 1-C_7H_{14} PPFs, while section 3.2 discusses the effects of partial premixing on the flame structure and NO emissions. Results concerning the effect of the fuel molecular structure on NO emission and the contributions of various NO formation routes are discussed in sections 3.3 and 3.4, respectively. Conclusions are presented in the last section.

2. NUMERICAL METHOD

The counterflow flame configuration employed in the present investigation is shown schematically in Figure 2. It consists of two opposing jets issuing from two coaxial nozzles that are placed one above the other. A rich fuel−air mixture flows from the lower nozzle, and air flows from the upper nozzle. The separation distance between the nozzles is 1.5 cm. The fuel inlet temperature is 400 K, while the oxidizer temperature is 300 K. PPFs are established for the two fuels by independently varying the fuel stream equivalence ratio (ϕ) and the global strain rate,[21] which is expressed as

$$a_G = \frac{2v_o}{L}\left(1 + \frac{v_f\sqrt{\rho_f}}{v_o\sqrt{\rho_o}}\right) \quad (1)$$

where L denotes the separation distance between the two jets, v_f denotes the fuel jet inlet velocity, v_o denotes the oxidizer jet inlet velocity, and ρ_f and ρ_o denote the mixture densities in the fuel and oxidizer streams, respectively. The inlet velocities of the fuel and oxidizer streams are specified by matching the momenta of the two streams for given ϕ and a_G. During this investigation, the strain rate is maintained at 100 s^{-1}.

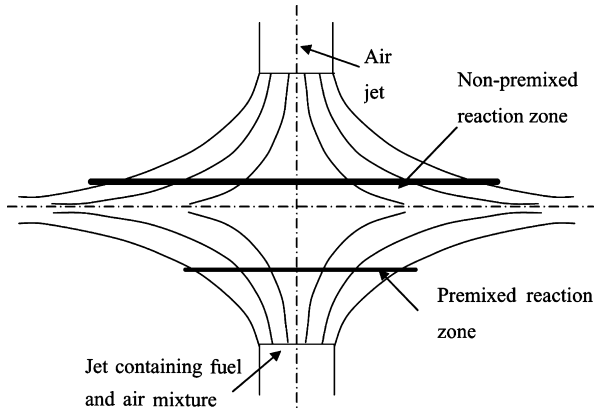

Figure 2. Schematic of the opposed jet PPF configuration.

Simulations were performed using the OPPDIF and CHEMKIN packages.[22,23] OPPDIF is a FORTRAN program that computes the flow field in a counterflow configuration using the numerical procedure as described in the cited reference. To establish grid independence, solutions were obtained on increasingly finer grids and by changing GRAD and CURV parameters until no variation was observed between two grid systems. The kinetic mechanism used to model *n*-heptane and 1-heptene flames has been developed previously by extending a detailed oxidation scheme for several fuels.[24,25] Because of the hierarchical modularity of the mechanistic scheme, the model is based on a detailed submechanism of C_1−C_4 species. Assuming analogy rules for similar reactions, only a few fundamental kinetic parameters are required for the progressive extension of the scheme toward heavier species. Simulations account for thermal radiation through an optically thin model.[26] The NO_x mechanism was adopted from various sources. The thermal NO formation is modeled using the extended Zeldovich mechanism.[27] The prompt NO mechanism is that proposed by Glarborg et al.,[28] while the intermediate N_2O mechanism is that reported by Malte and Pratt.[29] The NNH mechanism is adopted from the study by Smallwood et al.[19,20] Validation of the NO_x mechanism can be found in publications reported by Shimizu et al.[30] and Frassoldati et al.[31] The resulting kinetic model of hydrocarbon oxidation from methane up to *n*-octane consists of about 170 species and 5000 reactions. Numerical calculations are performed for *n*-heptane and 1-heptene PPFs with an equivalence ratio ranging from 2 to ∞.

3. RESULTS AND DISCUSSION

3.1. Validation of the Numerical Model and PPF Structure. While the kinetic mechanism has been extensively validated in previous studies, we provide an additional validation here using the measurements by Berta et al.[23] for a *n*-heptane PPF established at ϕ = 4.27, a_G = 100 s^{-1}, and nitrogen dilution of 17%. Figure 3 presents the predicted and measured temperature and species mole fraction profiles. There is good qualitative agreement between predictions and measurements, especially with respect to major (*n*-C_7H_{16}, O_2, and CO_2) and intermediate (CO, H_2, and C_2H_2) species profiles, with peak mole fractions of C_2H_4, C_2H_2, and CH_4 slighted overpredicted. In addition, the peak temperature is underpredicted, although radiation corrections are applied. It is important to note in this context that Berta et al.[23] reported measurements for several flames, and the comparison to these data indicated that the above case corresponds to the maximum temperature difference among the many flames analyzed. For other flames, the discrepancy between the measured and predicted flame temperatures was between 50 and 100 K, which was generally within the measurement uncertainty.

dx.doi.org/10.1021/ef2014315 | *Energy Fuels* 2012, 26, 879−888

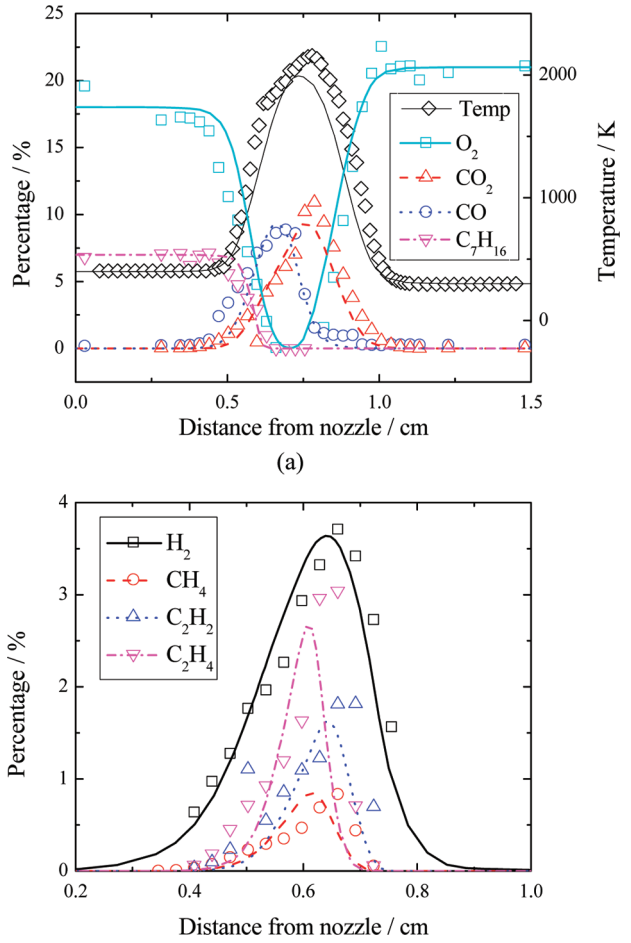

Figure 3. Predicted (lines) and measured[23] (symbols) flame structures in terms of temperature (◇) and species mole fraction profiles for *n*-heptane PPF at $\phi = 4.27$, $a_G = 100\ s^{-1}$, and nitrogen dilution of 17%: (a) (◇) temperature, (□) O_2, (△) CO_2, (○) CO, and (▽) *n*-C_7H_{16} profiles and (b) (□) H_2, (○) CH_4, (△) C_2H_2, and (▽) C_2H_4 profiles.

Table 1. Conditions for the Five Simulated *n*-Heptane and 1-Heptene Flames

	ϕ	$\Phi = 1 - 1/\phi$	fuel (%)	air (%)	N_2 dilution (%)
1	2	0.5	3	80	17
2	4	0.75	6	77	17
3	8	0.88	11	72	17
4	20	0.95	23	60	17
5	∞	1	83	0	17

To examine the effect of the chemical structure of the fuel and partial premixing, flames at different equivalence ratios were simulated using *n*-heptane and 1-heptene fuels. Table 1 lists the five flames in terms of ϕ analyzed in the present study. Here, $\phi = 2$, 4, and 8 correspond to PPFs, while $\phi = 20$ and ∞ represent diffusion flames. For all of the flames, the fuel stream was introduced from the bottom nozzle and the oxidizer was introduced from the top nozzle. The oxidizer was pure air, while the fuel stream was a mixture of fuels, air, and N_2 with the desired value of ϕ and N_2 dilution. Flames at different strain rates (a_G) and N_2 dilution will be investigated in a future study. Figure 4 presents the computed PPF structures, in terms of the temperature and species mole fraction profiles, for *n*-heptane and 1-heptene at $\phi = 2$. The corresponding profiles for *n*-heptane and 1-heptene flames at $\phi = \infty$ are shown in Figure 5. The global flame structure at a given ϕ is essentially the same for the two fuels. For both of the fuels, the flame at $\phi = 2$ contains a double flame structure. A rich premixed zone is established downstream of the fuel nozzle and characterized by fuel pyrolysis and partial oxidation. The products of partial oxidation, such as CO, H_2, and C_2H_2, are transported and consumed in the non-premixed reaction zone, which is located near the stagnation plane. The global structure for the diffusion flame ($\phi = \infty$) is also similar for the two fuels. As indicated in Figure 5, the diffusion flame for both of the fuels is located on the oxidizer side of the stagnation. Note, however, that in comparison to 1-heptene flames, the *n*-heptane flames produce a greater amount of H_2, CH_4, and C_2H_4 but a smaller amount of C_2H_2. This aspect is further discussed in the next section.

3.2. Partial Premixing Effect. Figure 6 presents the axial velocity profiles for the three *n*-heptane and 1-heptene flames established at $\phi = 2$, 4, and ∞. As expected in the context of the foregoing discussion, the velocity profiles at a given ϕ are quite similar for the two fuels. The two reaction zones for the PPFs at $\phi = 2$ and 4 are indicated by the peaks in the velocity profiles, with the rich premixed zone and non-premixed zone located on the fuel and oxidizer sides of the stagnation plane, respectively. As ϕ is increased, i.e., the level of partial premixing reduced, the rich premixed zone becomes progressively weaker and moves closer to the stagnation plane and the spatial separation between the two reaction zones deceases. In the limit (as ϕ goes to ∞), the rich premixed reaction zone becomes extinguished and the non-premixed reaction zone or the diffusion flame is located on the oxidizer side.

Figure 7 presents the temperature, C_2H_2, and NO mole fraction profiles for *n*-heptane flames established at $\phi = 2$, 4, and ∞. The corresponding results for 1-heptene flames at $\phi = 2$ and ∞ are shown in Figures 8 and 9, respectively. For both of the *n*-heptane and 1-heptene flames, as ϕ is increased, the C_2H_2 mole fraction increases, which can be attributed to the increase in the fuel mole fraction in the fuel stream. However, the peak NO exhibits a non-monotonic variation with ϕ, first increasing as ϕ is increased from 2 to 4 and then continuously decreasing as ϕ is increased toward the diffusion flame limit. Further analysis presented later in the paper indicated that the above behavior is attributed to how the NO formation because of different NO submechanisms varies with ϕ. Note that the thermal NO decreases monotonically ϕ, because the peak temperature location moves farther away from the stagnation plane, implying shorter residence time, as ϕ is increased. In addition, the extent of the high-temperature region is reduced at higher ϕ, which also leads to lower NO. This behavior is consistent with the results reported by Berta et al.[32] for *n*-heptane flames.

3.3. Effect of the Fuel Molecular Structure. The effect of the double bond in the fuel molecular structure on NO and C_2H_2 formation is depicted in Figure 10, which plots the peak mole fractions of C_2H_2, NO, and CH versus the parameter $\Phi = (1 - 1/\phi)$ for various *n*-heptane and 1-heptene flames. The use of parameter Φ facilitates representing the entire equivalence ratio range from $\phi = 2$ ($\Phi = 0.5$) to $\phi = \infty$ ($\Phi = 1$) analyzed in this study. As indicated, for all of the PPFs simulated, the peak NO mole fraction in 1-heptene flames is higher than that in *n*-heptane flames. This is consistent with the observation that the peak C_2H_2 is higher in 1-heptene flames compared to that in *n*-heptane flames, with the implication that the increased NO may be attributed to a higher amount of prompt NO formed in 1-heptene flames. Thus, the results seem to support the

dx.doi.org/10.1021/ef2014315 | *Energy Fuels* 2012, 26, 879–888

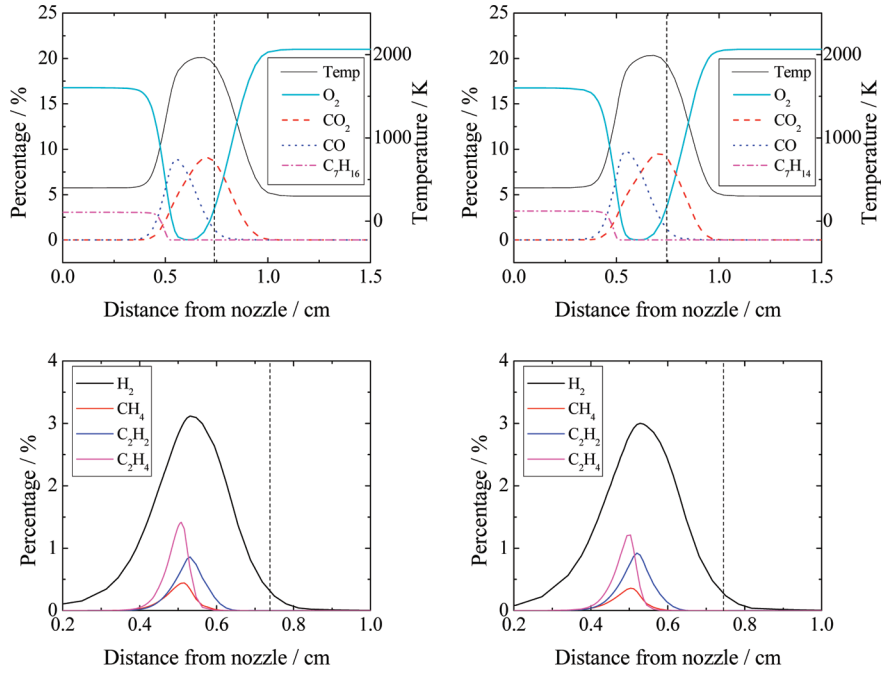

Figure 4. Flame structure in terms of the temperature and species mole fraction profiles for *n*-heptane (on the left) and 1-heptene (on the right) PPFs at $\phi = 2$, $a_G = 100\ s^{-1}$, and nitrogen dilution of 17%. The dashed vertical line indicates the stagnation plane location.

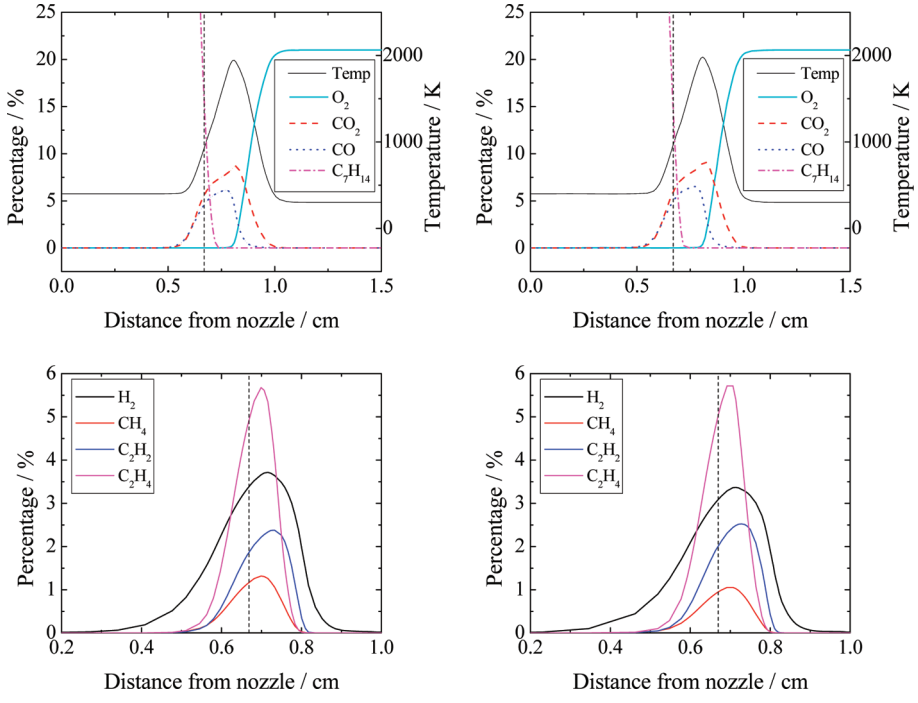

Figure 5. Flame structure in terms of the temperature and species mole fraction profiles for *n*-heptane (on the left) and 1-heptene (on the right) non-premixed flames ($\phi = \infty$) established at $a_G = 100\ s^{-1}$ and nitrogen dilution of 17%. The dashed vertical line indicates the stagnation plane location.

hypothesis that the increased NO associated with the combustion of biodiesel fuels may be related to the presence of double bonds in the fuel chemical structure. In addition, Figure 10 indicates that the difference between the peak NO values for the two fuels varies non-monotonically as the level of partial premixing is reduced or as Φ is increased. For Φ between 0.5 and 0.75 (or ϕ between 2 and 4), this difference increases, while the peak NO for both of the fuels also increases. As Φ is increased further toward the diffusion flame limit, the difference as well as the peak NO for the two fuels continuously decreases. A further discussion on this aspect is presented later in the context of Figures 12−15.

The prompt NO mechanism is driven by the CH radical formed from acetylene during combustion through the following reactions:[16,33]

$$C_2H_2 + O \rightarrow CH_2 + CO \quad (2)$$

dx.doi.org/10.1021/ef2014315 | *Energy Fuels* 2012, 26, 879−888

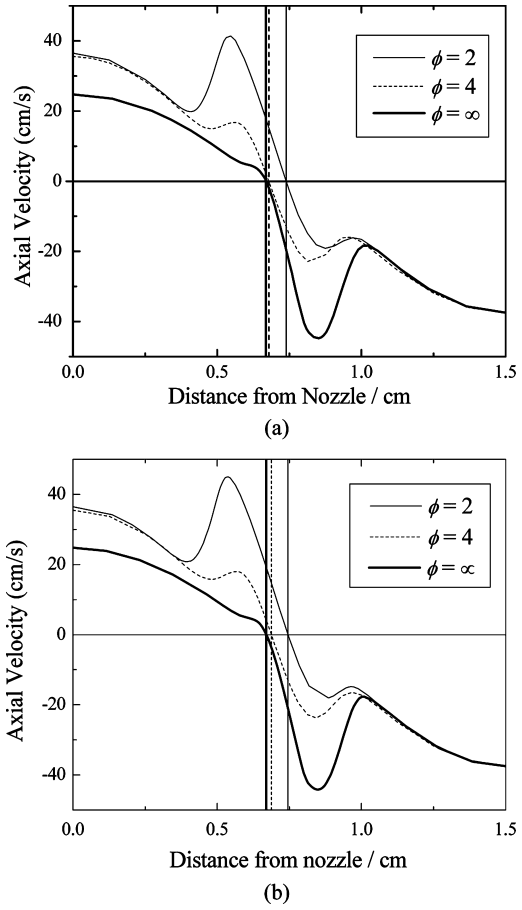

Figure 6. Axial velocity profiles for the three (a) *n*-heptane flames and (b) 1-heptene flames established at ϕ = 2 (thin line), ϕ = 4 (dash line), and ϕ = ∞ (thick line). The stagnation plane locations for the three flames are shown by vertical lines.

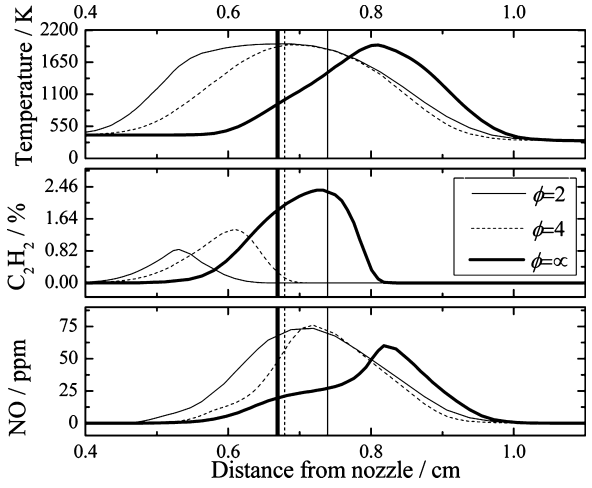

Figure 7. Temperature, C_2H_2, and NO mole fraction profiles for *n*-heptane flames established at ϕ = 2 (solid line), ϕ = 4 (dash line), ϕ = ∞ (thick line). Vertical lines indicate stagnation plane locations for the three flames.

$$H + CH_2 \rightarrow CH + H_2 \quad (3)$$

$$OH + CH_2 \rightarrow CH + H_2O \quad (4)$$

The CH radical then leads to the formation of NO through a complex set of reactions, which depends upon the structure of

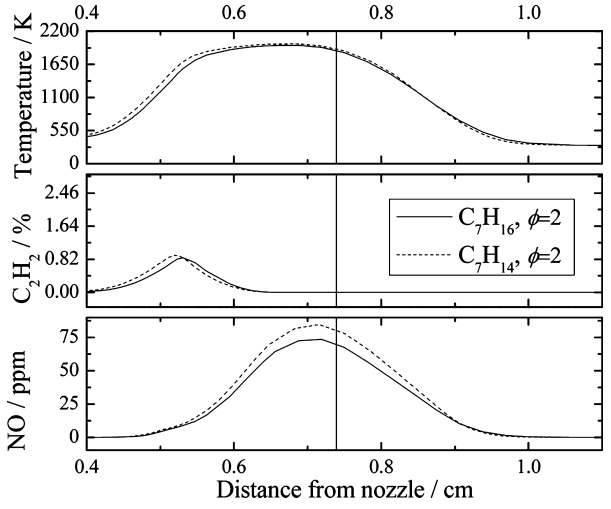

Figure 8. Temperature, C_2H_2, and NO mole fraction profiles for *n*-heptane (solid lines) and 1-heptene (dash lines) flames at equivalence ratio ϕ = 2. Vertical lines indicate stagnation planes for the two flames.

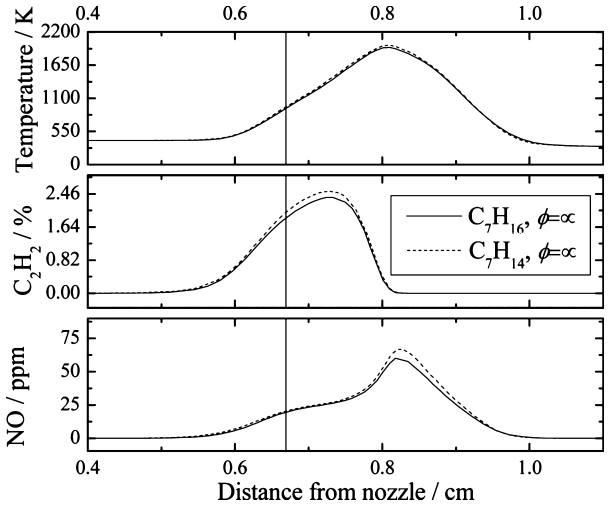

Figure 9. Temperature, C_2H_2, and NO mole fraction profiles for *n*-heptane (solid lines) and 1-heptene (dash lines) flames at ϕ = ∞. Vertical lines indicate stagnation planes for the two flames.

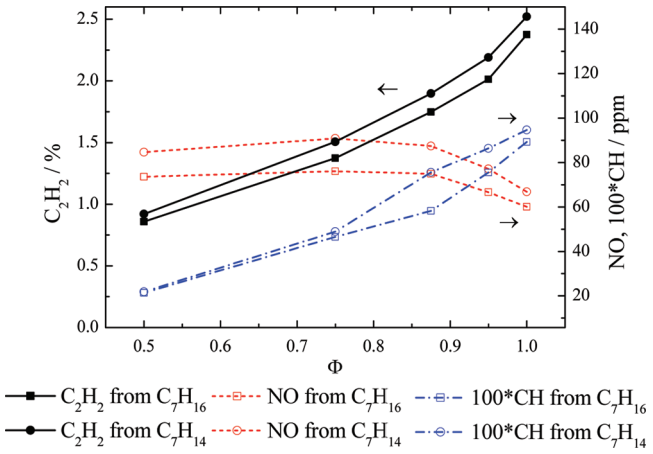

Figure 10. Peak values of C_2H_2, NO, and 100*CH plotted versus $\Phi = 1 - 1/\phi$, where Φ from 0.5 to 1.0 corresponds to the five cases listed in Table 1. The square and circle symbols indicate species for *n*-heptane and 1-heptene flames, respectively.

dx.doi.org/10.1021/ef2014315 | *Energy Fuels* 2012, 26, 879–888

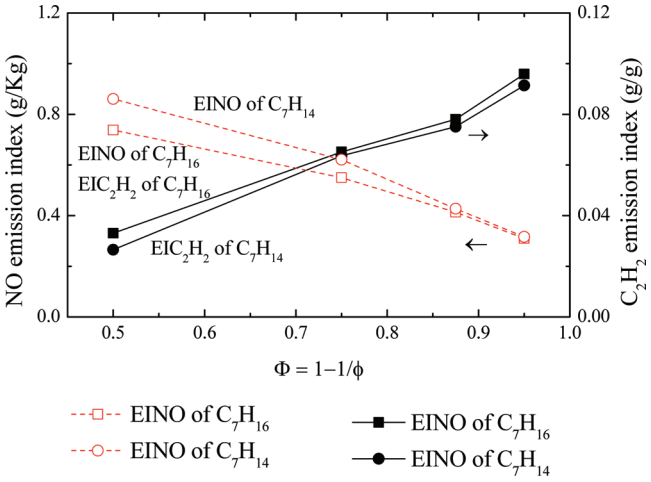

Figure 11. Emission index of NO and C_2H_2 plotted versus $\Phi = 1 - 1/\phi$, where Φ from 0.5 to 1.0 corresponds to the five cases listed in Table 1.

the starting fuel.[16] The following reactions, however, give an idea of how NO is formed, and these reactions are among the various pathways responsible for NO formation because of acetylene and CH production:

$$CH + N_2 \rightarrow NCN\ (\text{or}\ HCN) + H\ (\text{or}\ N) \quad (5)$$

$$CH_2 + N_2 \rightarrow HCN + NH \quad (6)$$

$$C + N_2 \rightarrow NCN \quad (7)$$

The first reaction dominates this sequence and produces NCN and H, which can yield NO through the following reactions:

$$NCN + O \rightarrow N + NCO \quad (8)$$

$$NCN + H \rightarrow HCN + N \quad (9)$$

$$NCN + H \rightarrow N + H_2 \quad (10)$$

$$NCO + O \rightarrow CN + NO \quad (11)$$

$$N + OH \rightarrow NO + H \quad (12)$$

The CH drives the formation of NCN, which in turn produces NO. The formation of CH depends upon CH_2, which is generally formed from C_2H_2, with C_2H_2 being the dominant source under fuel-rich conditions relevant to diesel engine combustion. For a more detailed description of reaction pathways appropriate to methyl esters, see ref 16.

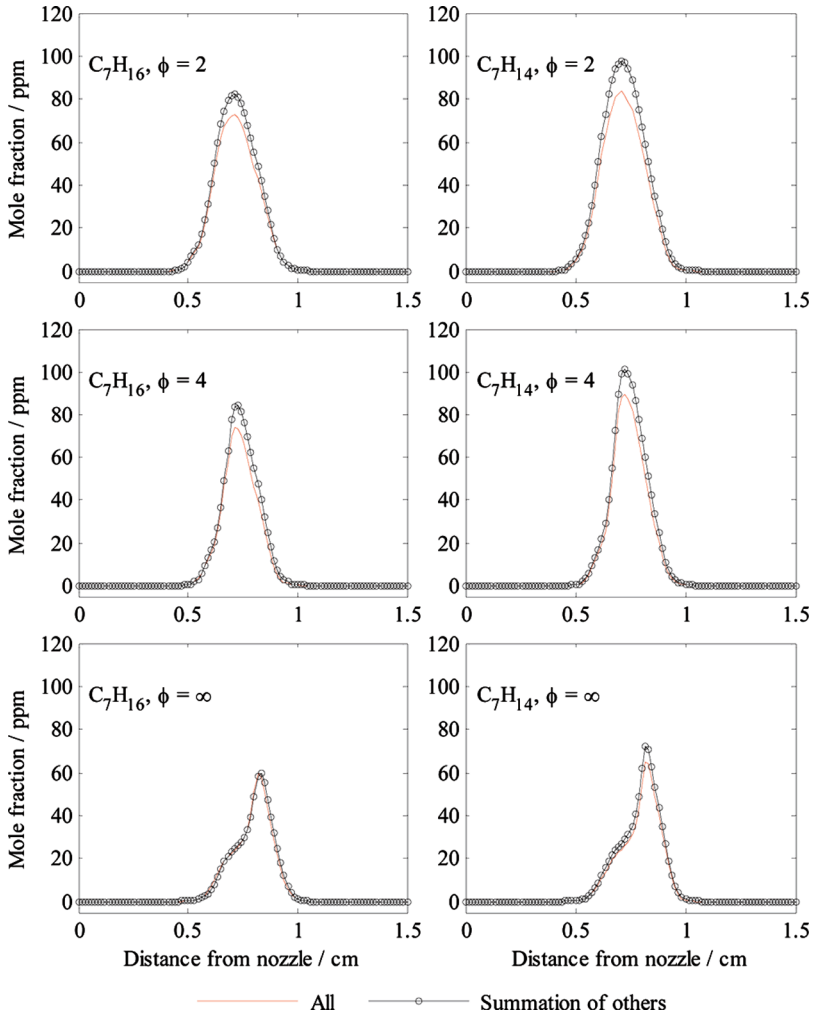

Figure 12. NO mole fraction profiles computed using the complete NO mechanism (red solid lines) and summing the contributions of the thermal, prompt, NNH, and N_2O intermediate routes (black lines with circle symbols). Results are shown for *n*-heptane and 1-heptene flames at ϕ = 2, 4, and ∞.

dx.doi.org/10.1021/ef2014315 | *Energy Fuels* 2012, 26, 879–888

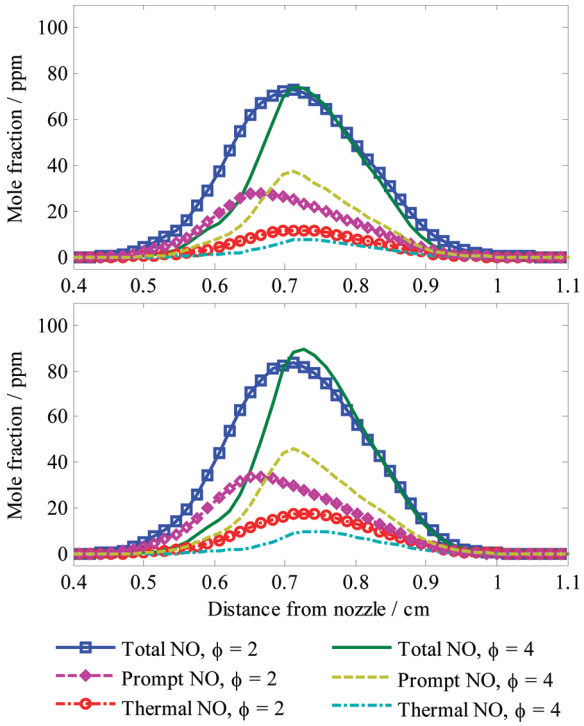

Figure 13. NO profiles computed using the complete NO, thermal NO, and prompt NO mechanisms for *n*-heptane and 1-heptene flames at $\phi = 2$ (symbols) and $\phi = 4$ (lines).

An alternative route through the formation of HCN[34] also depends upon C_2H_2 being the dominant source of CH_2 that leads to the formation of CH, as does a pathway involving HCNN.[16] Additionally, the evidence of C_2H_2 being the dominant source of CH_2 under rich combustion conditions has been provided by the rate of production analysis[35] for *n*-heptane PPFs.[36,18] Consequently, the presence of acetylene in the pyrolysis products can be used as an indicator of how different fuel structures may potentially affect NO_x levels. The presence of a double bond in unsaturated hydrocarbons, such as 1-heptene, promotes β-scission reactions, leading to higher acetylene formation.[33,16]

During the β-scission and NO formation, the presence of O_2 is important because it drives reactions through the path of forming a N atom, which may explain the higher amount of NO in 1-heptene PPFs. In contrast, long-chain saturated hydrocarbons, such as *n*-heptane, have lower probability to undergo β-scission, because the absence of the double bond leads to a more uniform distribution of electrons among all of the bonds. Consequently, fuels with a higher iodine number can be expected to produce a higher amount of NO_x in PPFs. As noted earlier in the context of Figure 10, the difference in the amount of NO formed for the *n*-heptane and 1-heptene flames decreases as the level of partial premixing is reduced, which is consistent with the lower probability of β-scission reactions for unsaturated fuels and at higher ϕ.

A global and perhaps better comparison of the emission characteristics of the two fuels is provided by an emission index. The NO_x emission index, EINO, is defined as

$$\mathrm{EINO} = \frac{\int_0^L \mathrm{MW_{NO}}\dot{\omega}_{\mathrm{NO}}\mathrm{d}x}{-\int_0^L \mathrm{MW_{fuel}}\dot{\omega}_{\mathrm{fuel}}\mathrm{d}x} \quad (13)$$

where MW represents the molecular weight, $\dot{\omega}$ represents the reaction rate (mol cm^{-3} s^{-1}), L represents the separation distance between the two nozzles, and x represents the axial coordinate. Figure 11 presents emission indices of NO and C_2H_2 plotted versus $\Phi = 1 - 1/\phi$. The EINO decreases as the level of partial premixing is reduced or ϕ is increased. In addition, the EINO for 1-heptene is higher than that for *n*-heptane, and the difference decreases as ϕ is increased, indicating that the effect of the fuel chemical structure on NO formation becomes less noticeable for diffusion flames compared to that for PPFs. It is also interesting to note some differences between the variations of peak NO and EINO with respect to the equivalence ratio. As indicated in Figures 10 and 11, the peak NO varies non-monotonically, while EINO decreases monotonically with the increase in ϕ.

3.4. Contributions of Various NO Formation Routes.

As discussed in previous studies,[18−20] the prompt NO is a major contributor to the total NO_x for long-chain hydrocarbons, such as *n*-heptane. To examine the relative contributions of various NO routes, simulations were performed for each of the four NO routes, namely, the thermal, prompt, N_2O intermediate, and NNH routes.[19,20] For instance, the thermal NO_x route includes the following reactions:

$$N_2 + O \rightarrow N + NO \quad (14)$$

$$N + OH \rightarrow NO + H \quad (15)$$

$$N + O_2 \rightarrow NO + O \quad (16)$$

The initiating reaction for thermal NO formation is reaction 14. Similarly, particular reactions associated with prompt NO include $CH + N_2 \rightarrow HCN + N$, $CH_2 + N_2 \rightarrow HCN + NH$, $C + N_2 \rightarrow CN + N$, $NH_2 + N \rightarrow N_2 + H + H$, $NH_2 + NO \rightarrow N_2 + H_2O$, $NH + NH \rightarrow N_2 + H + H$, $NCO + N \rightarrow N_2 + CO$, $N_2O + CO \rightarrow N_2 + CO_2$, $NCO + NCO \rightarrow CO + CO + N_2$, and $NCO + NO \rightarrow N_2 + CO_2$.

Reactions associated with the N_2O intermediate submechanism include $N_2 + O + M \rightarrow N_2O + M$, $N_2O + H \rightarrow N_2 + OH$, $N_2O + O \rightarrow N_2 + O_2$, and $N_2O + OH \rightarrow N_2 + HO_2$.

Similarly, reactions associated with the NNH submechanism are $NNH \rightarrow N_2 + H$, $N_2 + H_2 \rightarrow NNH + H$, $NNH + OH \rightarrow N_2 + H_2O$, $NNH + O_2 \rightarrow N_2 + HO_2$, $NNH + O_2 \rightarrow N_2 + H + O_2$, $NNH + NH \rightarrow N_2 + NH_2$, $NNH + NH_2 \rightarrow N_2 + NH_3$, $NNH + NO \rightarrow N_2 + HNO$, $HNNO + M \rightarrow N_2 + OH + M$, $NH + N \rightarrow N_2 + H$, and $NH + NO \rightarrow N_2 + OH$.

To compute the contribution of each NO formation route, four sets of simulations were performed. Figure 12 presents the NO profiles computed using the complete NO mechanism and summing the contributions of the four NO routes. In general, the total NO from the summation of the four routes exceeds that obtained using the complete NO mechanism, with the largest discrepancy (~15%) occurring near the stagnation plane for the 1-heptene PPF at $\phi = 2$. This is consistent with the results reported in previous studies[19,20] and may be attributed to the fact that removing certain reactions associated with a given NO submechanism may affect the mole fractions of species involved in another NO submechanism. Overall, the total NO obtained by summing the contributions of various NO routes is fairly close to that obtained using the complete NO mechanism.

Figure 13 presents NO profiles computed using the total NO, thermal NO, and prompt NO mechanisms for *n*-heptane and 1-heptene flames at $\phi = 2$ and 4. Results indicate that the

dx.doi.org/10.1021/ef2014315 | *Energy Fuels* 2012, 26, 879−888

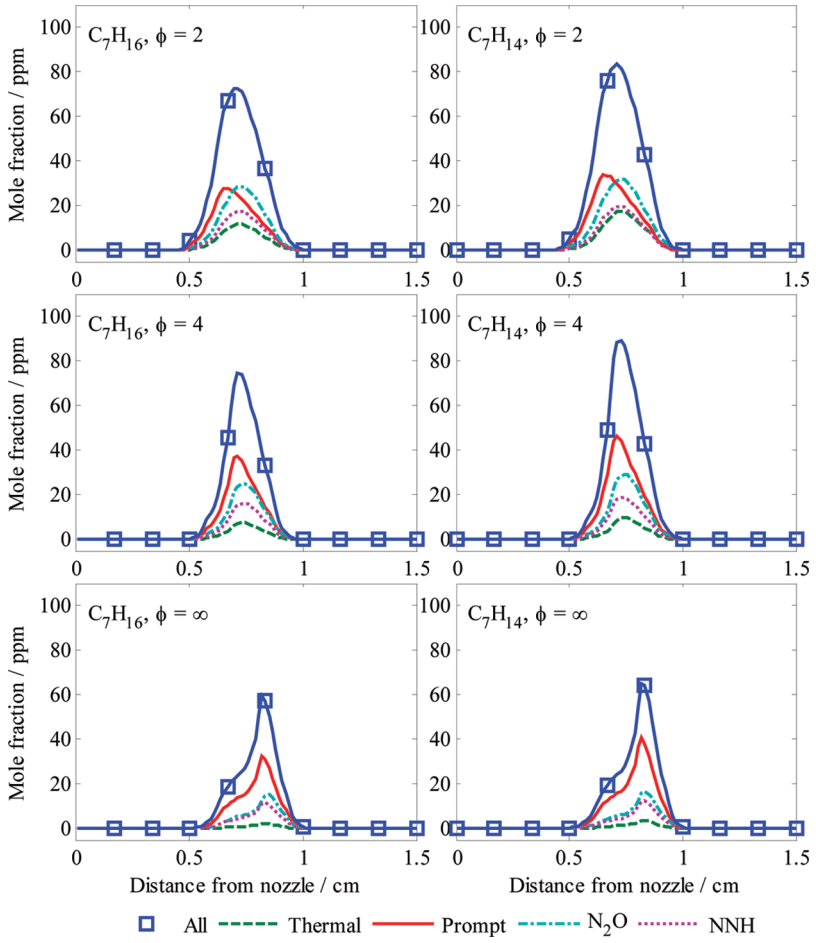

Figure 14. NO profiles computed using the complete NO_x mechanism and using the thermal, prompt, N_2O intermediate, and NNH submechanisms for *n*-heptane and 1-heptene flames established at ϕ = 2, 4, and ∞. Blue solid line with square symbols represents the complete NO_x mechanism, while the dashed, solid, dash-dotted, and dotted lines represent the thermal, prompt, N_2O intermediate, and NNH submechanisms, respectively.

Table 2. Peak Flame Temperature and Peak NO (Given in ppm and %) Formed with the Complete NO Mechanism and through the Thermal, Prompt, N_2O Intermediate, and NNH Routes for the Three *n*-Heptane and 1-Heptene Flames at Different Equivalence Ratios

variable	*n*-heptane flames			1-heptene flames		
equivalence ratio (ϕ)	2	4	∞	2	4	∞
peak temperature (K)	1967	1948	1945	1993	1987	1981
total NO (ppm)	72.7	74.3	59.5	83.5	89.3	65.0
thermal NO (ppm)	11.8 (16%)	7.7 (10%)	2.4 (4%)	17.5 (21%)	9.8 (11%)	3.9 (6%)
prompt NO (ppm)	27.8 (38%)	37.1 (50%)	32.4 (54%)	33.7 (40%)	46.0 (51%)	40.7 (63%)
N_2O intermediate NO (ppm)	28.6 (39%)	25.2 (34%)	15.2 (26%)	32.1 (38%)	29.3 (33%)	16.6 (26%)
NNH intermediate NO (ppm)	17.6 (24%)	16.3 (22%)	11.6 (19%)	19.5 (23%)	19.0 (21%)	12.3 (19%)

contribution of thermal NO to the total NO is relatively small in these flames. In addition, as ϕ is increased, the contribution of thermal NO decreases, while that of prompt NO increases. The comparison of the relative contributions of the four submechanisms is presented in Figure 14, which plots the NO profiles for the complete NO mechanism and for four submechanisms for *n*-heptane and 1-heptene flames at ϕ = 2, 4, and ∞. The peak NO values and peak temperature for each of these mechanisms are also listed in Table 2. In addition, the peak NO values for the various mechanisms are shown in Figure 15. These results indicate that the prompt NO provides the largest contribution to the total NO in these flames, followed by the intermediate N_2O, NNH, and thermal NO mechanisms. Thus, the prompt NO contributes 28−37% and 33−46% in *n*-heptane and 1-heptene flames, respectively, depending upon the level of partial premixing. The corresponding values for other three mechanisms are 12−18% and 12−20% for intermediate N_2O, 15−29% and 17−32% for NNH, 2−12% and 4−18% for thermal in *n*-heptane and 1-heptene flames, respectively. Another important observation

dx.doi.org/10.1021/ef2014315 | *Energy Fuels* 2012, 26, 879−888

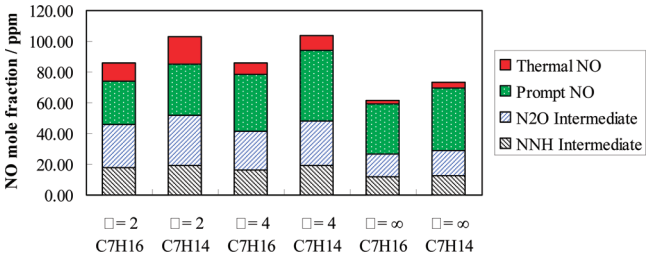

Figure 15. Contribution of each submechanism to total NO in terms of the peak NO mole fraction for *n*-heptane and 1-heptene flames at ϕ = 2, 4, and ∞.

is that the relative contribution of prompt NO to total NO is higher in 1-heptene flames compared to that in *n*-heptane flames. Finally, it should be noted from Table 2 that the flame temperature for 1-heptene is typically 30−40 K higher than that for *n*-heptane, which partly contributes to the increased NO for 1-heptene.

4. CONCLUSION

PPFs burning *n*-heptane and 1-heptene fuels in an opposed jet configuration have been simulated to examine the hypothesis that the increased NO_x from the combustion of biodiesel fuel components can be related to the presence of double bonds in the fuel chemical structure. These two fuels represent the hydrocarbon side chain of the two surrogate biodiesel esters, methyl octanoate (C9:0) and methyl octenoate (C9:1), respectively. The computational model has been validated using previously reported measurements of PPFs. The NO_x emission for the two fuels is characterized in terms of the NO_x profiles and emission index for different levels of partial premixing. Important observations are as follows: (1) The β-scission and oxidation reactions related to the C═C double bond lead to a higher amount of C_2H_2 and, thus, increased NO through the prompt mechanism in 1-C_7H_{14} flames compared to that in *n*-C_7H_{16} flames. However, differences in the amount of NO formed for the two fuels generally become less pronounced as the level of partial premixing is reduced or the equivalence ratio is increased toward the diffusion flame limit (ϕ = ∞). (2) The peak NO exhibits a non-monotonic variation with respect to ϕ. It first increases as ϕ is increased from 2 to 4 and then decreases as ϕ is increased toward the diffusion flame. In contrast, the NO emission index decreases monotonically with the increase in ϕ. (3) The variation of peak NO with ϕ for the prompt mechanism follows a similar behavior as that indicated by the total NO. However, the peak NO values for the N_2O intermediate, NNH, and thermal mechanisms decrease monotonically with the increase in ϕ. (4) Analysis of the various NO production pathways indicate that the total NO formed is mainly due to the prompt and intermediate N_2O mechanisms, followed by the NNH and thermal NO mechanisms.

Future work will focus on performing experiments and simulations of these flames using long-chain saturated and unsaturated biodiesel components, such as methyl octanoate and methyl octenoate, for a range of equivalence ratios and strain rates.

AUTHOR INFORMATION

Corresponding Author

*Telephone: 312-996-2235. Fax: 312-413-0441 E-mail: ska@uic.edu.

Notes

The authors declare no competing financial interest.

ACKNOWLEDGMENTS

This research was partially supported by the Combustion and Plasma Systems Division, National Science Foundation, through Award CTS-0553439.

REFERENCES

(1) Graboski, M. S.; McCormick, R. L. *Prog. Energy Combust. Sci.* **1998**, *24*, 125−164.
(2) McCormick, R. L.; Graboski, M. S.; Alleman, T. L.; Herring, A. M. *Environ. Sci. Technol.* **2001**, *35*, 1742−1747.
(3) McCormick, R. L.; Williams, A.; Ireland, J.; Brimhall, M.; Hayes, R. R. *Effects of Biodiesel Blends on Vehicle Emissions*, Milestone Report; National Renewable Energy Laboratory (NREL): Golden, CO, 2006; NREL/MP-540-40554, data taken from *A Comprehensive Analysis of Biodiesel Impacts on Exhaust Emissions*, Draft Technical Report, 2002; EPA420-P-02-001.
(4) National Renewable Energy Laboratory (NREL). *Biodiesel Handling and User Guide*; NREL: Golden, CO, 2009; NREL/TP-540-43672.
(5) Mueller, C.; Cheng, E.; Boehman, A. An introduction to biodiesel. *SNL CRF News* **2006**, *28* (May/June), 3.
(6) Stotler, R.; Human, D. *Transient Emission Evaluation of Biodiesel Fuel Blend in a 1987 Cummins L-10 and DDC 6V-92-TA*; National Biodiesel Board: Jefferson City, MO, Nov 30, 1995; ETS Report ETS-95-128.
(7) Sharp, C. A. *Transient Emissions Testing of Biodiesel in a 6V-92TA DDEC Engine*; National Biodiesel Board: Jefferson City, MO, Oct 1994; Southwest Research Institute Report 6602 and 6673.
(8) Graboski, M. S.; McCormick, R. L.; Alleman, T. L. *The Effect of Biodiesel Composition on Engine Emissions from a DDC Series 60 Diesel Engine*; National Renewable Energy Laboratory (NREL): Golden, CO, 2003; NREL/SR-520-31461.
(9) Curran, H. J.; Pitz, W. J.; Westbrook, C. K. *NC7_2b Mechanism. UCRL-WEB-204236 Release*, May 19, 2004; http://www.cms.llnl.gov/combustion/.
(10) Smith, G. P.; Golden, D. M.; Frenklach, M.; Moriarty, N. W.; Eiteneer, B.; Goldenberg, M.; Bowman, C. T.; Hanson, R. K.; Song, S.; Gardiner, W. C.; Lissianski, V. V., Jr.; Qin, Z. *GRI-MECH 3.0*; http://www.me.berkeley.edu/gri_mech/.
(11) Fisher, E. M.; Pitz, W. J.; Curran, H. J.; Westbrook., C. K. *Proc. Combust. Inst.* **2000**, *28*, 1579−1586.
(12) Marchese, A. J.; Angioletti, M.; Dryer, F. L. Flow reactor studies of surrogate biodiesel fuels. *Proceedings of the 30th International Symposium on Combustion*; Chicago, IL, July 2004.
(13) Metcalfe, W.; Dooley, W.; Curran, H., Simmie, J. An experimental and chemical kinetic modeling study of surrogate diesel fuels. *Proceedings of the 6th International Chemical Kinetics Conference*; National Institute of Standards and Technology (NIST), Gaithersburg, MD, July 2005; Paper H2.
(14) Sarathy, S. M.; Gail, S.; Thomson, M. J.; Dagaut, P. *Proc. Combust. Inst.* **2007**, *31*, 1015−1022.
(15) Garner, S.; Sivaramakrishnan, R.; Brezinsky, K. *Proc. Combust. Inst.* **2009**, *32*, 461−467.
(16) Garner, S.; Brezinsky, K. *Combust. Flame* **2011**, *158*, 2289−2301.
(17) Garner, S.; Dubois, T.; Togbe, C.; Chaumeix, N.; Dagaut, P.; Brezinsky, K. *Combust. Flame* **2011**, *158*, 2302−2313.
(18) Naha, S.; Aggarwal, S. K. *Combust. Flame* **2004**, *139*, 90−105.
(19) Guo, H.; Smallwood, G. J. *Combust. Theory Modell.* **2007**, *11*, 741−753.
(20) Guo, H.; Smallwood, G. J. *Int. J. Therm. Sci.* **2007**, *46*, 936−943.
(21) Fisher, E. M.; Williams, B. A.; Fleming, J. W. *Proc. East. States Sect. Combust. Inst.* **1997**, 191−194.
(22) Lutz, A. E.; Kee, R. J.; Grcar, J. F.; Rupley, F. M. *OPPDIF: A FORTRAN Program for Computing Opposed Flow Diffusion Flames*;

Sandia National Laboratories: Livermore, CA, 1997; Technical Report SAND 96-8243, UC-1404.
(23) Berta, P. Numerical and experimental investigation of *n*-heptane combustion in a counterflow configuration. Ph.D. Thesis, University of Illinois at Chicago, Chicago, IL, 2005.
(24) Ranzi, E.; Dente, M.; Goldaniga, A.; Bozzano, G.; Faravelli, T. *Prog. Energy Combust. Sci.* **2001**, *27*, 99−139.
(25) Goldaniga, A.; Faravelli, T.; Ranzi, E. *Combust. Flame* **2000**, *122*, 350−358.
(26) Pogliani, B.; Bundy, M.; Hamins, A.; Puri, I. K. *Proceedings of the 2nd Joint Technical Meeting of the U.S. Sections of the Combustion Institute*; Oakland, CA, March 25−28, 2001; Paper 218.
(27) Zeldovich, J. *Acta Physicochim. URSS* **1946**, *21*, 577−628.
(28) Glarborg, P.; Jensen, A. D.; Johnsson, J. E. T. *Prog. Energy Combust.* **2003**, *29*, 89−113.
(29) Malte, P.; Pratt, D. T. *Proc. Combust. Inst.* **1974**, *15*, 1061−1070.
(30) Shimizu, T.; Williams, F. A.; Frassoldati, A. *Proceedings of the 43rd American Institute of Aeronautics and Astronautics (AIAA) Aerospace Sciences Meeting and Exhibit*; Reno, NV, Jan 10−13, 2005; AIAA-0144.
(31) Frassoldati, A.; Faravelli, T.; Ranzi, E. *Combust. Flame* **2003**, *135*, 97−112.
(32) Berta, P.; Aggarwal, S. K.; Puri, I. K. *Combust. Flame* **2006**, *145*, 740−764.
(33) Garner, S. Biologically derived diesel fuel and NO_x formation: An experimental and kinetic modeling study of saturated and unsaturated C8 fatty acid methyl esters. Ph.D. Thesis, University of Illinois at Chicago, Chicago, IL, 2011.
(34) Miller, J. A.; Bowman, C. T. *Prog. Energy Combust. Sci.* **1989**, *15*, 287−337.
(35) Turanyi, T. *KINALC*; http://www.chem.leeds.ac.uk/Combustion/kinalc.html.
(36) Xue, H.; Aggarwal, S. K. *Combust. Flame* **2003**, *132*, 723−741.